Generalized oscillator strengths and integral cross sections for the valence-shell excitations of oxygen studied by fast electron impact

Wei-Qing Xu, Jian-Min Sun,* You-Yan Wang, and Lin-Fan Zhu†
Hefei National Laboratory for Physical Sciences at Microscale, Department of Modern Physics, University of Science and Technology of China, Hefei, Anhui 230026, China
(Received 16 July 2010; published 25 October 2010)

The generalized oscillator strengths and differential cross sections for electron-impact excitation of the $A'\,^3\Delta_u$, Schumann-Runge continuum, and $E\,^3\Sigma_u^-(v'=0,1)$ states of oxygen have been determined at an incident electron energy of 2.5 keV. Good agreement is found between the present generalized oscillator strengths of the Schumann-Runge continuum and $E\,^3\Sigma_u^-(v'=1)$ states and the previous ones measured at higher impact energies, which indicates that the first Born approximation is satisfied at an impact energy of 400 eV. However, the large difference between the present generalized oscillator strengths of the $A'\,^3\Delta_u$ and $E\,^3\Sigma_u^-(v'=0)$ states and the previous ones is observed, and the possible reasons are discussed. The *BE*-scaled (binding energy *B* and excitation energy *E*) or *BEf*-scaled (*B*, *E*, and *f* values) integral cross sections for the $A'\,^3\Delta_u$, Schumann-Runge continuum, and $E\,^3\Sigma_u^-(v'=0,1)$ states from its threshold to 5 keV were calculated based on the present generalized oscillator strengths. The present scaled integral cross sections are in good agreement with the previous ones measured at the moderate impact energies except for that of the $A'\,^3\Delta_u$ state.

DOI: 10.1103/PhysRevA.82.042716 PACS number(s): 34.80.Gs, 33.70.Ca, 33.70.Fd, 34.50.Bw

I. INTRODUCTION

Oxygen, the second most abundant composition in Earth's atmosphere, plays an important role in a variety of combustion and energy conversion processes. In the life sciences it is a key element in respiration. In addition, the processes of the dissociation and predissociation of oxygen by the absorption of solar radiation are significant in atmospheric phenomena such as aurora and dayglow [1,2]. So the accurate knowledge of the absolute differential cross sections (DCSs) and generalized oscillator strengths (GOSs) for the valence shell excitations of O_2 is of great importance in many areas such as atmospheric physics, life sciences, radiation physics, astrophysics, etc. [3]. On the other hand, from the viewpoint of pure physics and chemistry, the relative vibrational intensity distribution for the transition of $E\,^3\Sigma_u^- \leftarrow X\,^3\Sigma_g^-$ in O_2 violates the Franck-Condon principle, which is caused by the strongly avoided crossing of two potential energy curves corresponding to a Rydberg and a valence state of $^3\Sigma_u^-$ symmetry [4–7]. Therefore, the study of the DCSs and GOSs of O_2 will provide new insight into the avoided crossing of potential curves and anomalous behavior of intensity distribution within a vibrational progression.

According to the nonrelativistic Born approximation, the GOS is defined as (in atomic units) [8–11]:

$$f(E_n,K)=\frac{E_n}{2}\frac{p_0}{p_a}K^2\frac{d\sigma_n}{d\Omega}=\frac{2E_n}{K^2}\left|\langle\Psi_n|\sum_{j=1}^{N}e^{i\vec{\mathbf{K}}\cdot\vec{\mathbf{r}}_j}|\Psi_0\rangle\right|^2. \quad (1)$$

Here, $f(E_n,K)$ and $d\sigma_n/d\Omega$ stand for the GOS and DCS, while Ψ_0 and Ψ_n are the N-electron wave functions for the initial and final states, respectively. E_n and K are the excitation energy and momentum transfer, while p_0 and p_a are the incident and scattered electron momenta, respectively. $\vec{\mathbf{r}}_j$ is the position vector of the jth atomic electron.

The DCSs and integral cross sections (ICSs) of the Herzberg pseudocontinuum, which consists of the $A\,^3\Sigma_u^+$, $c^1\Sigma_u^-$, and $A'\,^3\Delta_u$ states, were extensively studied by electron impact at low and moderate incident energies [12–19] and well summarized by Brunger and Buckman [3]. Among them, Trajmar *et al.* [12] reported the DCSs and ICSs of the Herzberg pseudocontinuum at the incident electron energies of 20 and 45 eV, and they pointed out that the Herzberg pseudocontinuum is dominated by a spin exchange process at these impact energies. Wakiya [13] made a comprehensive investigation on the DCSs and ICSs of the Herzberg pseudocontinuum for the incident electron energies from 20 to 500 eV and scattering angles from 5° to 130°. This work shows that the Herzberg pseudocontinuum is dominated by the electron exchange excitation of $c^1\Sigma_u^- \leftarrow X\,^3\Sigma_g^-$ at the low collision energies (<100 eV), while it is dominated by the direct excitation of $A\,^3\Sigma_u^+ + A'\,^3\Delta_u \leftarrow X\,^3\Sigma_g^-$ for the high collision energies (>100 eV). The joint experimental and theoretical work of Teillet-Billy *et al.* [14] studied the ICSs of the Herzberg pseudocontinuum and shows that there is an $O_2^-(^2\Pi_g)$ resonance at about 8 eV in the excitation process of the Herzberg pseudocontinuum. Allan [15] observed a broad feature in the ICSs whose absolute values are reasonably consistent with those of Tellit-Billy *et al.* [14]. Campbell *et al.* [16] reported the DCS and ICS of $A\,^3\Sigma_u^+ + c^1\Sigma_u^- + A'\,^3\Delta_u$ at an incident electron energy of 15 eV, then Green *et al.* [17,18] extended the DCS and ICS measurement of the Herzberg pseudocontinuum to seven incident electron energies in the range of 9–20 eV. Shyn and Sweeney [19] reported the DCSs and ICSs for the individual $A\,^3\Sigma_u^+$, $c^1\Sigma_u^-$, and $A'\,^3\Delta_u$ states at the incident electron energies from 10 to 30 eV. However, because of lacking peak profile information of the $A\,^3\Sigma_u^+$, $c^1\Sigma_u^-$, and $A'\,^3\Delta_u$ states, the DCSs and ICSs of Shyn and Sweeney [19] suffer the randomicity from the

*Present address: Institute for Theoretical Physics, School of Physics and Electronics, Henan University, Kaifeng, Henan 475004, China.
†lfzhu@ustc.edu.cn.

spectral deconvolution procedure, which was also pointed out by Green *et al.* [17]. As for the theoretical works, using the R-matrix method, Noble and Burke [20] and Higgins *et al.* [21] calculated the ICSs of the Herzberg pseudocontinuum for the incident electron energies less than 15 eV, and their results also show the existence of the resonance structure in the ICS of the Herzberg pseudocontinuum. However, the experimental results of Teillt-Billy *et al.* [14], Allan [15], and Green *et al.* [17] did not give the explicit evidence about the resonant structure.

As for the Schumann-Runge continuum and $E\ ^3\Sigma_u^-(v'=0,1)$, there are relatively fewer DCSs and GOSs measurements by electron-impact excitation. The DCSs, GOSs, and ICSs of the Schumann-Runge continuum were measured by Trajmar *et al.* [12], Lassettre *et al.* [22], Wakiya [23], Newell *et al.* [24], and Shyn *et al.* [25] at the incident electron energies of 20–45, 519, 20–500, 100–500, and 15–50 eV, respectively. As for the electron-impact excitation of the $E\ ^3\Sigma_u^-(v'=0,1)$ states, their DCSs, GOSs, and ICSs were measured by Trajmar *et al.* [12], Newell *et al.* [24], and Shyn *et al.* [26] at the incident electron energies of 20–45, 100–500, and 15–50, respectively. To the best of our knowledge, only Li *et al.* [4] and Dillon *et al.* [6] calculated the GOSs of the $E\ ^3\Sigma_u^-(v'=0,1)$ states versus K^2.

The vibrational intensity distribution of the $E\ ^3\Sigma_u^-$ state of O_2 violates the Franck-Condon principle, which has attracted extensive attention [4–7]. Dillon *et al.* [6] determined the experimental GOS ratios f_{10}/f_{00} of the $E\ ^3\Sigma_u^-$, $v'=1$ and 0 in the region of $0<K^2<1$ a.u. at the incident electron energies of 200 and 400 eV, and their results show that the f_{10}/f_{00} sharply decreases as K^2 increases in this K^2 region. In order to explain the behavior, using the multireference single- and double-excitation configuration interaction method (MRD-CI), Li *et al.* [4] calculated the GOSs of some vibrational transitions of $E\ ^3\Sigma_u^- \leftarrow X\ ^3\Sigma_g^-$. Employing the Born approximation combined with the MRD-CI method, Kimura *et al.* [5] and Dillon *et al.* [6] calculated the generalized transition moment (GTM) for the $E\ ^3\Sigma_u^- \leftarrow X\ ^3\Sigma_g^-$ transition in $0<K^2<1$ a.u., and the GOS ratios for $E\ ^3\Sigma_u^-$, $v'=0$ and 1 were obtained by integrating the products of vibrational overlap functions and GTM. As an extension to the work of Dillon *et al.* [6], Lewis *et al.* [7] extended the concept of the GTM beyond the region of applicability of the first Born approximation (FBA), and using the coupled-channel method they explained unusual vibrational intensity distributions of many features in the 7–11.2 eV energy loss region. The previous investigations [4–7] show that the anomalous behavior of vibrational intensity distribution of the $E\ ^3\Sigma_u^-$ state can be attributed to a strong avoided crossing of two potential curves corresponding to the Rydberg and valence states with $^3\Sigma_u^-$ symmetry, respectively, due to the strong interaction between them.

According to the above survey, most of the previous works concentrate on the low or moderate impact energies. The present work extends the experimental study to the higher impact energy of 2.5 keV, and the DCSs, GOSs, and ICSs for the $A'\ ^3\Delta_u$, Schumann-Runge continuum, and $E\ ^3\Sigma_u^-(v'=0,1)$ states, as well as the vibrational intensity distribution of the $E\ ^3\Sigma_u^-$ state, were reported. In the following sections, the experimental apparatus and procedures will be given in Sec. II. Then, the results and discussions will be presented in Sec. III.

II. EXPERIMENTAL APPARATUS AND PROCEDURES

The GOSs and DCSs of O_2 were measured by an angle-resolved electron-energy-loss spectrometer, which was described in detail in our previous works [27,28]. For this experiment, the impact energy was set at 2.5 keV and the energy resolution was about 100 meV. The background pressure in the vacuum chamber was 5×10^{-5} Pa. The true zero angle was calibrated by the symmetry of the angular distribution of the inelastic scattering signals of the transition of $E\ ^3\Sigma_u^-(v'=0) \leftarrow X\ ^3\Sigma_g^-$ around the geometry nominal 0°.

The method of gas mixture (O_2 and He with a fixed proportion) used in this work was described in detail in our previous works [29,30]. Briefly, the electron-energy-loss spectra were recorded from 1.0° to 8.5° with an interval of 0.5°. A typical electron-energy-loss spectrum is shown in Fig. 1, and the excited states are assigned. In order to determine the intensities of the $A'\ ^3\Delta_u$ state of O_2 (herein the contributions from the transition of $c^1\Sigma_u^-$ and $A\ ^3\Sigma_u^+ \leftarrow X\ ^3\Sigma_g^+$ can be neglected, which will be discussed in Sec. III), the least-squares fitting method was used to deconvolve the measured spectra. The spectra in the energy region of 4–9 eV were fitted by four Gaussian functions, one of which was used to fit the $A'\ ^3\Delta_u$ state. The contribution of the Schumann-Runge continuum to the $A'\ ^3\Delta_u$ state was considered by the other three Gaussian peaks. After the intensity of the $A'\ ^3\Delta_u$ state was determined, the fitted Gaussian function of the $A'\ ^3\Delta_u$ state was subtracted from the spectra. Then, the intensities of the Schumann-Runge continuum and $E\ ^3\Sigma_u^-(v'=0,1)$ states were obtained by directly integrating the regions of 6.56–9.46, 9.76–10.17, and 10.17–10.44 eV, respectively. As for the intensity of the $2\ ^1P$ of helium, it was obtained by deducting a linear background in the fitted results. It should be pointed out that the $2\ ^1P$ of helium is overlapped with the $(2\sigma_u)^{-1}3s\sigma$ state of O_2 [31,32]. However, since the $(2\sigma_u)^{-1}3s\sigma$ of O_2 is a shallow window resonance and the ratio of helium to oxygen is about 2 in the mixed gas, the error of the intensity of $2\ ^1P$

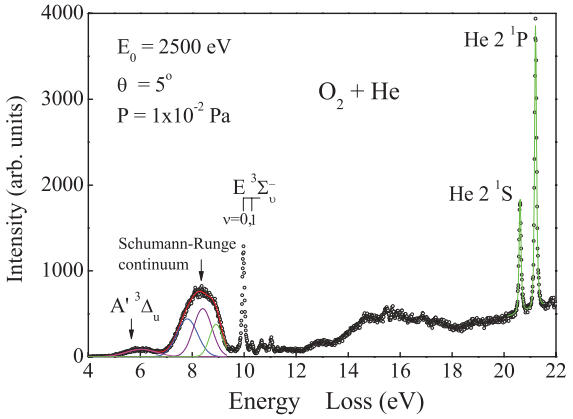

FIG. 1. (Color online) A typical electron-energy-loss spectrum of O_2 and He at the incident energy of 2.5 keV and scattering angle of 5°. The fitted results are shown as lines.

of helium induced by the $(2\sigma_u)^{-1}3s\sigma$ state should be less than 5%.

After the intensities of the $A'\,^3\Delta_u$, the Schumann-Runge continuum and $E\,^3\Sigma_u^-(v'=0,1)$ of O_2, as well as that of the $2\,^1P$ of helium, were obtained, the influences of the double scattering and the angular resolution, which had been described in detail in our previous works [27,30,33,34], were corrected. Then, the known DCS of the $2\,^1P$ of helium calculated by Han and Li [35], which is in excellent agreement with our previous experimental result [36], is used to calibrate the variable collision length at the different scattering angle. The relative DCS for the individual excitation of O_2 was determined through multiplying the ratio of the intensity of the transition of O_2 to that of the $2\,^1P$ of helium by the DCS of the $2\,^1P$ of helium calculated by Han and Li [35].

Applying with Eq. (1), the relative DCSs for the transitions of O_2 were converted into the relative GOSs. Based on the Lassettre's limit theorem [37,38] that the GOS converges to the optical oscillator strength (OOS) as $K^2 \to 0$, the relative GOS can be converted into the absolute one by normalizing the extrapolated value at $K^2 = 0$ to the absolute OOS of the transition.

Based on the analytic properties identified by Lassettre and his coworkers [37,38], the GOS can be represented by [37–40]

$$f(E_n,K) = \frac{x^M}{(1+x)^{(l+l'+M+5)}} \sum_{m=0}^{\infty} \frac{f_m x^m}{(1+x)^m}, \tag{2}$$

where $x = K^2/\alpha^2$ with $\alpha = (2I)^{1/2} + [2(I-E_n)]^{1/2}$, and I and E_n are the ionization and excitation energies, respectively. l and l' are the orbital angular momenta of the initial and final states of the target electron, while M is an integer which is relevant to the transition multipolarity [39,40] and f_m are the fitting parameters. For a dipole-allowed transition, $M = 0$ and f_0 is the OOS. Since the ionization energy I of an electron in a molecule is defined only in the context of a simply independent particle model by Lassettre [37] and a GOS is calculated from multiconfiguration wave function, it is better to simply take α^2 as a fitting parameter along with f_m as proposed by Kim [41].

By fitting the relative GOS of the excitation of the Schumann-Runge continuum using the above Lassettre formula and normalizing the fitted parameter f_0 (relative OOS) to the absolute one (0.169) determined by the dipole (e,e) method [42], the absolute GOS and the fitted result of the Schumann-Runge continuum were obtained. The relative GOSs for electron-impact excitation of the $A'\,^3\Delta_u$ and $E\,^3\Sigma_u^-(v'=0,1)$ states were converted into absolute ones through multiplying them by the same scale factor used to determine the absolute GOS for the Schumann-Runge continuum. Then, the absolute GOSs of the $A'\,^3\Delta_u$ and $E\,^3\Sigma_u^-(v'=0,1)$ were fitted by the above Lassettre formula.

From the fitted results using the Lassettre formula, the ICSs for the electron-impact excitation of the $A'\,^3\Delta_u$, Schumann-Runge continuum and $E\,^3\Sigma_u^-(v'=0,1)$ states can be calculated (in atomic units) [8]:

$$\sigma_{\rm Born}^n(E_0) = \frac{\pi}{E_0 E_n} \int_{K_{\rm min}^2}^{K_{\rm max}^2} \frac{f(K,E_n)}{K^2} dK^2, \tag{3}$$

with

$$K_{\rm min}^2 = [\sqrt{2E_0} - \sqrt{2(E_0-E_n)}]^2, \tag{4}$$

and

$$K_{\rm max}^2 = [\sqrt{2E_0} + \sqrt{2(E_0-E_n)}]^2. \tag{5}$$

Where $\sigma_{\rm Born}^n(E_0)$ stands for the ICS of an excited state n at an incident electron energy E_0, $K_{\rm min}$ and $K_{\rm max}$ represent the minimum and maximum momentum transfers, respectively.

Recently, Kim [41,43] developed *BE* scaling and *BEf* scaling approaches in calculating ICSs for dipole-allowed excitations in atoms and molecules. *BE*-scaled $[\sigma_{BE}(T)]$ and *BEf*-scaled $[\sigma_{BEf}(T)]$ ICSs are written as

$$\sigma_{BE}(T) = \frac{T}{T+B+E}\sigma_{\rm Born}(T), \tag{6}$$

$$\sigma_{BEf}(T) = \frac{f_{\rm accu}}{f_{\rm Born}}\sigma_{BE}(T), \tag{7}$$

where $\sigma_{\rm Born}(T)$ is the Born cross section at an incident energy T, B is the binding energy of the electron being excited, E is the excitation energy, $f_{\rm accu}$ is an accurate OOS value, while $f_{\rm Born}$ is the f value obtained from the same set of wave functions used in calculating the Born cross section.

The experimental errors of the GOSs in this work are estimated at about 15%, including the contributions from the statistics of counts, the angular resolution and angle determination, the pressure correction, the normalizing procedure, as well as the deconvolution procedure. Among them, the error from the deconvolution procedure is the main part for the GOS of the $A'\,^3\Delta_u$ at the small scattering angles because of its very weak intensity. The error of the normalizing procedure is 7% including the error of the OOS of the Schumann-Runge continuum [42] and the one of the fitting procedure using Eq. (2). For most cases, the errors of the pressure correction are less than 7%, in which the errors of the statistics of counts and those of the deconvolution procedure are included. The errors from the angular resolution and angle determination are 2%−12% according to the different scattering angles. The uncertainties of the present ICSs are about 20%. The overall experimental errors are shown in the corresponding figures.

III. RESULTS AND DISCUSSIONS

A. GOSs for the $A'\,^3\Delta_u$, Schumann-Runge continuum, and $E\,^3\Sigma_u^-(v'=0,1)$ states in O_2

The absolute GOS and DCS values for electron-impact excitation of the $A'\,^3\Delta_u$, Schumann-Runge continuum, and $E\,^3\Sigma_u^-(v'=0,1)$ states are listed in Table I, and the GOSs are shown in Figs. 2–5 along with the previous experimental and theoretical results as well as the presently fitted curves by the Lassettre formula.

From Fig. 1 it can be seen that a broad peak locates in the energy region of 4.6–6.8 eV, which corresponds to the transition of $A'\,^3\Delta_u \leftarrow X\,^3\Sigma_g^-$. In the previous studies at low or moderate collision energies [12–19], a similar feature, which corresponds to the Herzberg pseudocontinuum of $A\,^3\Sigma_u^+ + c^1\Sigma_u^- + A'\,^3\Delta_u$, was also observed. Compared with the previous investigations, the peak in the presently measured spectra only comes from the contribution of the

TABLE I. The GOSs and DCSs for the $A'^3\Delta_u$, Schumann-Runge continuum, and $E\ ^3\Sigma_u^-(v'=0,1)$ states in O_2. Square brackets denote the power of ten.

	GOS				DCS (a_0^2 sr^{-1})			
K^2 (a.u.)	$A'^3\Delta_u$	$S-R$[a]	$E(v'=0)$[b]	$E(v'=1)$[c]	$A'^3\Delta_u$	$S-R$[a]	$E(v'=0)$[b]	$E(v'=1)$[c]
0.07		1.46[−1]	1.10[−2]	6.97[−3]		1.37[+1]	8.57[−1]	5.26[−1]
0.14		1.32[−1]	1.15[−2]	5.54[−3]		6.18	4.48[−1]	2.09[−1]
0.23		1.02[−1]	1.04[−2]	4.32[−3]		2.91	2.46[−1]	9.92[−2]
0.36	5.35[−4]	8.42[−2]	1.21[−2]	3.40[−3]	1.32[−2]	1.53	1.83[−1]	4.99[−2]
0.51	7.50[−4]	6.83[−2]	1.13[−2]	2.55[−3]	1.31[−2]	8.77[−1]	1.21[−1]	2.64[−2]
0.70	9.76[−4]	5.32[−2]	9.94[−3]	1.90[−3]	1.24[−2]	4.98[−1]	7.74[−2]	1.43[−2]
0.91	1.43[−3]	4.60[−2]	9.22[−3]	1.58[−3]	1.40[−2]	3.31[−1]	5.52[−2]	9.17[−3]
1.14	2.00[−3]	3.45[−2]	7.00[−3]	1.29[−3]	1.56[−2]	1.98[−1]	3.35[−2]	5.98[−3]
1.41	1.99[−3]	2.81[−2]	5.64[−3]	7.78[−4]	1.26[−2]	1.31[−1]	2.18[−2]	2.91[−3]
1.70	2.18[−3]	2.28[−2]	4.31[−3]	7.24[−4]	1.14[−2]	8.79[−2]	1.38[−2]	2.25[−3]
2.02	2.14[−3]	1.74[−2]	3.39[−3]	4.55[−4]	9.44[−3]	5.64[−2]	9.15[−3]	1.19[−3]
2.37	2.19[−3]	1.45[−2]	2.53[−3]	4.20[−4]	8.23[−3]	4.01[−2]	5.82[−3]	9.36[−4]
2.74	1.98[−3]	1.11[−2]	1.82[−3]	3.63[−4]	6.44[−3]	2.65[−2]	3.62[−3]	6.70[−4]
3.15	1.68[−3]	8.64[−3]	1.33[−3]	2.55[−4]	4.75[−3]	1.80[−2]	2.30[−3]	4.28[−4]
3.58	1.51[−3]	7.11[−3]	1.01[−3]	2.22[−4]	3.76[−3]	1.30[−2]	1.54[−3]	3.27[−4]
4.04	1.41[−3]	5.51[−3]	8.13[−4]	1.71[−4]	3.11[−3]	8.93[−3]	1.10[−3]	2.24[−4]

[a] $S-R$, [b] $E(v'=0)$, and [c] $E(v'=1)$ are short for the Schumann-Runge continuum, the $E\ ^3\Sigma_u^-(v'=0)$ state, and the $E\ ^3\Sigma_u^-(v'=1)$ state, respectively.

$A'^3\Delta_u \leftarrow X\ ^3\Sigma_g^-$ transition. The reason can be elucidated as follows: Different from the low-energy electron impact, for sufficiently fast electron impact, the influence of the incident particle upon an atom or molecule can be regarded as a sudden and small external perturbation, and the probability for the spin-forbidden transition in connection with the electron-exchange effect is negligibly small for fast electron impact [8,16]. So the transition of $c^1\Sigma_u^- \leftarrow X\ ^3\Sigma_g^-$ can be neglected for the present incident electron energy of 2.5 keV. In addition, according to the selection rule for the $\Sigma^+ \leftrightarrow \Sigma^-$ transition in electron-molecule collisions [44], the transition probability of $A\ ^3\Sigma_u^+ \leftarrow X\ ^3\Sigma_g^-$ should be negligibly small for the small scattering angles, which pertains to the present scattering condition (i.e., the scattering angles are less than 8.5°). Therefore, compared with the previously measured DCSs of the $A\ ^3\Sigma_u^+ + c^1\Sigma_u^- + A'\ ^3\Delta_u$ by the low or moderate energy collision, the present work measured the GOS and DCS of the pure excitation of $A'\ ^3\Delta_u \leftarrow X\ ^3\Sigma_g^-$.

The present GOS of the $A'\ ^3\Delta_u$ state is shown in Fig. 2 along with the previous experimental results of Wakiya [13] measured at the collision energies from 100 to 500 eV. From Fig. 2 it can be seen that the present GOS for $A'\ ^3\Delta_u \leftarrow X\ ^3\Sigma_g^-$ increases for $K^2 < 2$ a.u., until it reaches a maximum at $K^2 \approx 2$ a.u., and then it decreases slowly for $K^2 > 2$ a.u.. It can also be seen that the apparent GOS measured by Wakiya [13] at an incident electron energy of 100 eV is in good agreement with ours, however, Wakiya's apparent GOSs measured at 150–500 eV are much higher than ours. It is well known that the apparent GOS approaches the GOS as the incident electron energy increases, so the agreement

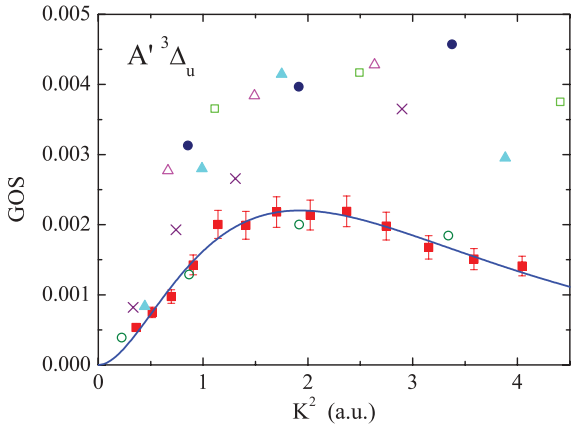

FIG. 2. (Color online) The GOS for the $A'\ ^3\Delta_u$ state in O_2. Solid (red) squares, the present result; solid (blue) line, fitted result. The results of Wakiya [13] at the incident electron energies are as follows: open (green) circles, 100 eV; crosses (purple), 150 eV; solid (turquoise) triangles, 200 eV; open (magenta) triangles, 300 eV; solid (blue) circles, 400 eV; open (green) squares, 500 eV.

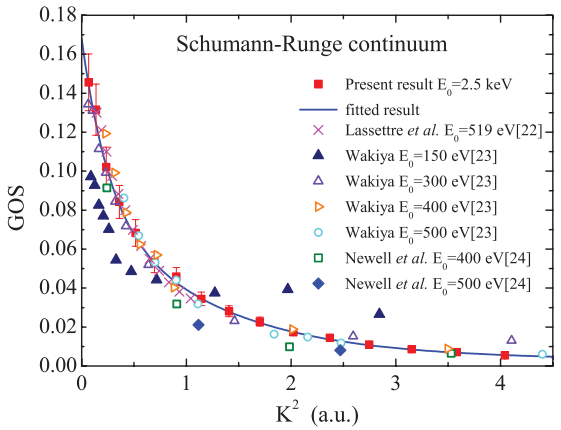

FIG. 3. (Color online) The GOS for the Schumann-Runge continuum in O_2.

between the apparent GOS of Wakiya [13] measured at 100 eV and the present one is occasional considering the large difference between the results of Wakiya [13] at 150–500 eV and the present one at 2.5 keV. The large discrepancies can not be attributed to the normalization procedure considering the good agreement between our result and the ones of Wakiya [13] for the Schumann-Runge continuum (see Fig. 3 and the discussion below). One possible reason may be the contamination of the Schumann-Runge continuum to the Herzberg pseudocontinuum in the work of Wakiya [13] since they determined DCSs by integrating the energy loss region of 4.5–7.1 eV, and the situation is more serious for the lower K^2 region because of the very weak intensity of the Herzberg pseudocontinuum. However, in our work this contamination is carefully considered in the fitting procedure. Another possible reason may be that the intensity of $A\,^3\Sigma_u^+ \leftarrow X\,^3\Sigma_g^-$ is comparable with or larger than that of $A'\,^3\Delta_u \leftarrow X\,^3\Sigma_g^-$ at the impact energies of 150–500 eV, while our result is the pure transition of $A'\,^3\Delta_u \leftarrow X\,^3\Sigma_g^-$.

The GOS of the Schumann-Runge continuum is shown in Fig. 3 along with the previous experimental data of Lassettre *et al.* [22] at 519 eV, Wakiya [23] at 150–500 eV, and Newell *et al.* [24] at 400–500 eV. It can be seen clearly from Fig. 3 that the GOS of the Schumann-Runge continuum decreases with the increasing of K^2, which is the typical character of a dipole-allowed transition. Figure 3 also shows that the present GOS is in excellent agreement with those of Wakiya [23] at 400–500 eV and Lassettre *et al.* [22] at 519 eV in the whole K^2 region, while the apparent GOS of Wakiya [23] at 300 eV is in good agreement with ours except that it is slightly larger than ours for $K^2 > 2$ a.u.. Therefore, the FBA is satisfied in the present measured K^2 region for the Schumann-Runge continuum at an impact energy of 400 eV. The deviation of the apparent GOS of Wakiya [23] at 150 eV from the other results means that the FBA is not valid at an impact energy of 150 eV. As for the results of Newell *et al.* [24] at 400 and 500 eV, they are generally lower than other results for $E_0 \geqslant 400$ eV. The difference between the results of Newell *et al.* [24] and other data may be attributed to the pressure effect. In fact, the pressure effect has been corrected in the present work and those of Lassettre *et al.* [22] as well as Wakiya [23], while Newell *et al.* [24] did not consider the effect.

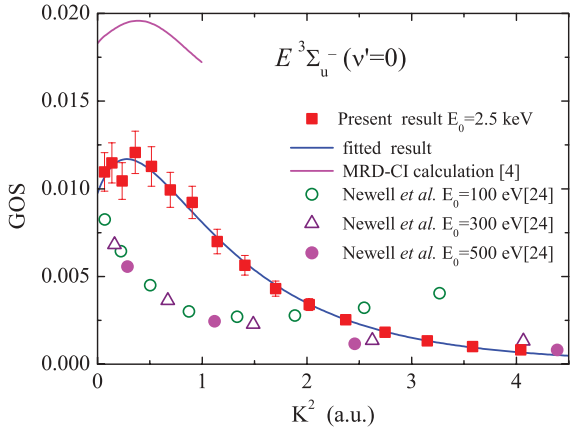

FIG. 4. (Color online) The GOS for the $E\,^3\Sigma_u^-(\nu' = 0)$ state in O_2.

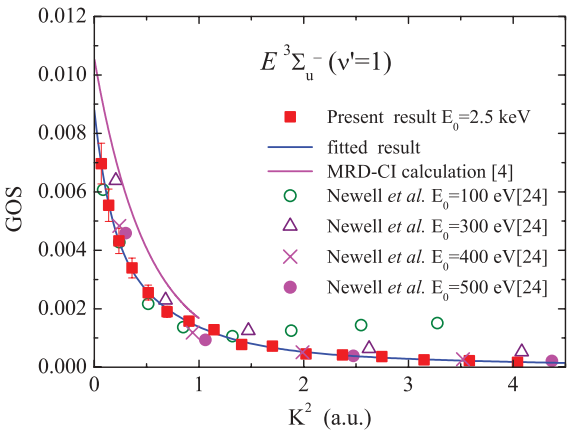

FIG. 5. (Color online) The GOS for the $E\,^3\Sigma_u^-(\nu' = 1)$ state in O_2.

The present GOSs for the transition of $E\,^3\Sigma_u^-(\nu' = 0,1) \leftarrow X\,^3\Sigma_g^-$ are shown in Figs. 4 and 5, respectively. From Fig. 4 it can be seen that the GOS of the $E\,^3\Sigma_u^-(\nu' = 0)$ state has a hump in the small K^2 region ($K^2 < 0.3$ a.u.), which was also predicted by the MRD-CI calculation based on the FBA [4]. However, the calculated GOS is much higher than the present result in absolute values. The experimental results of Newell *et al.* [24] measured at 100–500 eV are much lower than the present ones in $K^2 < 2$ a.u., and there is not the hump observed by their work. Although it is generally thought that the GOSs of the vibronic states from the same electronic state have the same or similar profile, the GOS of the $E\,^3\Sigma_u^-(\nu' = 1)$ state (i.e., which has not the hump and decreases quickly as the K^2 increases) shows a different profile from that of the $E\,^3\Sigma_u^-(\nu' = 0)$. However, the profile of our results for the $E\,^3\Sigma_u^-(\nu' = 1)$ state is in reasonable agreement with the MRD-CI calculation based on the FBA of Li *et al.* [4]. But our GOSs are lower than theirs in absolute values. The present GOS ratio of f_{10}/f_{00} is shown in Fig. 6 along with the previous experimental [6,24] and theoretical [6] works. From Fig. 6 it can be seen that the present f_{10}/f_{00} is in good agreement with the experimental ones of Dillon *et al.* [6] measured at the impact energies of 200 and 400 eV and the MRD-CI calculation [6], while

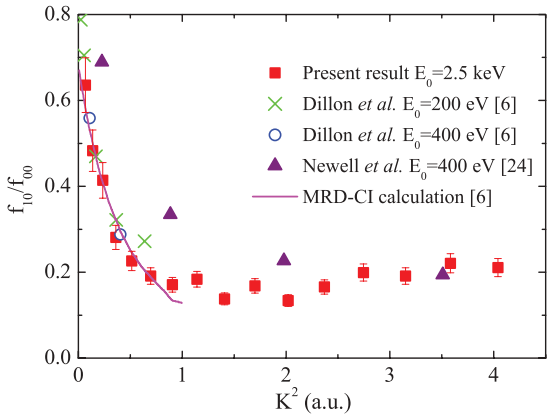

FIG. 6. (Color online) The GOS ratio for the $E\,^3\Sigma_u^-, \nu' = 0$ and $\nu' = 1$ states in O_2.

the GOS ratio of Newell *et al.* [24] converted from their experimental results at 400 eV is much higher than other experimental and theoretical [6] ones. Considering the good agreement of the GOS of the $E\ ^3\Sigma_u^-(v'=1)$ state between Newell *et al.* [24] and ours, the difference of the GOS ratio of f_{10}/f_{00} between the result of Newell *et al.* [24] and other experimental and theoretical results suggests that the GOS of the $E\ ^3\Sigma_u^-(v'=0)$ state of Newell *et al.* [24] may suffer some unknown errors. It should be emphasized that the discrepancy of the GOS of the $E\ ^3\Sigma_u^-(v'=0)$ state between Newell *et al.* [24] and the present work should not be attributed to the validity or not of the FBA, since the GOSs of the $E\ ^3\Sigma_u^-(v'=1)$ state and the Schumann-Runge continuum as well as the GOS ratio of f_{10}/f_{00} of the $E\ ^3\Sigma_u^-(v'=0,1)$ states measured at different incident electron energies show the good or reasonable agreement, while the Schumann-Runge continuum and $E\ ^3\Sigma_u^-(v'=0,1)$ states are formed by the same valence-Rydberg mixing [5–7].

B. ICSs for the $A'\ ^3\Delta_u$, Schumann-Runge continuum, and $E\ ^3\Sigma_u^-(v'=0,1)$ states in O_2

According to Eqs. (3)–(7), the *BE*- or *BEf*-scaled ICS for a transition can be calculated from the theoretical GOS or the reliable experimental GOSs [41,43]. For oxygen, to the best of our knowledge, there are no theoretical investigations about the GOSs of the $A'\ ^3\Delta_u$ and Schumann-Runge continuum states, and the calculated GOSs of the $E\ ^3\Sigma_u^-(v'=0,1)$ states [4,6] are limited to a narrow K^2 region. However, considering that the calculated GOS profiles of the $E\ ^3\Sigma_u^-(v'=0,1)$ states [6] are in good agreement with the present results and the present GOSs measured at a high-impact energy are in good agreement with the previous experimental results for the Schumann-Runge continuum [22,23] and $E\ ^3\Sigma_u^-(v'=1)$ [24] states, we have the confidence that the present GOSs of the $A'\ ^3\Delta_u$, Schumann-Runge continuum, and $E\ ^3\Sigma_u^-(v'=0,1)$ states are reliable. The present *BE*- or *BEf*-scaled ICSs for the

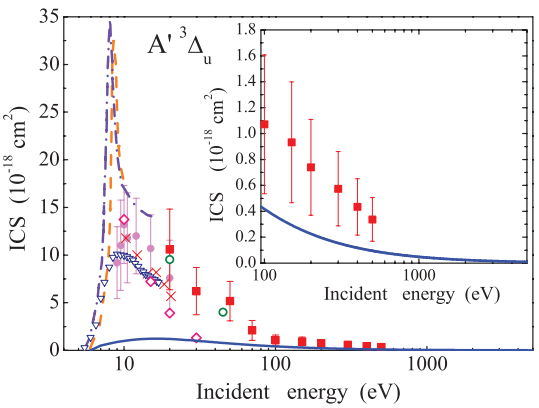

FIG. 7. (Color online) The ICS for the Herzberg pseudocontinuum in O_2. Solid (blue) line, the *BE*-scaled ICS. The experimental results are as follows: open (green) circles, Trajmar *et al.* [12]; solid (red) squares, Wakiya [13]; open (blue) triangles, Teillet-Billy *et al.* [14]; solid (purple) circles, Green *et al.* [17]; open (purple) diamonds, Shyn and Sweeney [19]. The theoretical results are as follows: crosses (red), Teillet-Billy *et al.* [14]; dashed-dotted-dashed (purple) line, Noble and Burke [20]; dashed (orange) line, Higgins *et al.* [21].

TABLE II. The *BE*- or *BEf*-scaled ICSs (10^{-18} cm^2) for the $A'\ ^3\Delta_u$, Schumann-Runge continuum, and $E\ ^3\Sigma_u^-(v'=0,1)$ states in O_2. Square brackets denote the power of ten.

E_0 (eV)	$A'\ ^3\Delta_u$ *BE*	$S-R$ *BE*	$E(v'=0)$ *BEf*	$E(v'=1)$ *BEf*
5.99	0			
6	4.47[−2]			
8.29	7.64[−1]	0		
9	8.74[−1]	1.84[+1]		
9.96	9.92[−1]	2.72[+1]	0	
10	9.94[−1]	2.75[+1]	4.38[−1]	
10.28	1.02	2.92[+1]	1.21	0
12	1.14	3.74[+1]	2.67	4.86[−1]
15	1.22	4.52[+1]	3.46	7.58[−1]
20	1.19	5.06[+1]	3.79	9.83[−1]
30	1.01	5.22[+1]	3.71	1.15
40	8.46[−1]	5.00[+1]	3.46	1.17
45	7.81[−1]	4.89[+1]	3.31	1.17
50	7.25[−1]	4.75[+1]	3.17	1.15
60	6.32[−1]	4.47[+1]	2.92	1.12
70	5.59[−1]	4.19[+1]	2.72	1.07
80	5.03[−1]	3.96[+1]	2.53	1.03
90	4.58[−1]	3.74[+1]	2.37	9.86[−1]
100	4.19[−1]	3.54[+1]	2.23	9.47[−1]
150	2.92[−1]	2.81[+1]	1.72	7.84[−1]
200	2.26[−1]	2.36[+1]	1.41	6.69[−1]
300	1.55[−1]	1.79[+1]	1.04	5.22[−1]
400	1.18[−1]	1.46[+1]	8.34[−1]	4.30[−1]
500	9.52[−2]	1.23[+1]	6.99[−1]	3.68[−1]
600	7.98[−2]	1.07[+1]	6.04[−1]	3.23[−1]
700	6.88[−2]	9.52	5.31[−1]	2.89[−1]
800	6.04[−2]	8.57	4.75[−1]	2.62[−1]
900	5.37[−2]	7.81	4.33[−1]	2.40[−1]
1000	4.86[−2]	7.19	3.96[−1]	2.21[−1]
1500	3.26[−2]	5.17	2.80[−1]	1.61[−1]
2000	2.45[−2]	4.07	2.19[−1]	1.28[−1]
2500	1.96[−2]	3.40	1.80[−1]	1.07[−1]
3000	1.63[−2]	2.92	1.54[−1]	9.21[−2]
4000	1.23[−2]	2.28	1.20[−1]	7.28[−2]
5000	9.83[−3]	1.88	9.83[−2]	6.04[−2]

$A'\ ^3\Delta_u$, Schumann-Runge continuum, and $E\ ^3\Sigma_u^-(v'=0,1)$ states are listed in Table II and shown in Figs. 7–10.

From Fig. 7, it can be seen that our *BE*-scaled ICSs of the $A'\ ^3\Delta_u$ state are much lower than all previous results [12–14,17,19–21] at the low-impact energies. This discrepancy can be easily understood since the previous ICSs have the contributions from the $A\ ^3\Sigma_u^+$ and $c^1\Sigma_u^-$ states, while the present ICSs come from the pure excitation of $A'\ ^3\Delta_u \leftarrow X\ ^3\Sigma_g^-$. In particular, the Herzberg pseudocontinuum is dominated by the spin-exchange transition of $c^1\Sigma_u^-$ at the low-impact energies (<100 eV), which was also pointed out by Wakiya [13]. However, it is somewhat strange that the ICSs of Wakiya [13] measured at the incident electron energies from 100 to 500 eV are larger than the present *BE*-scaled ICSs by a factor more than 2 since the ICSs of the Schumann-Runge continuum show a good agreement with ours for the incident electron energy region from 150 to 500 eV (see Fig. 8). The difference of the ICSs between the

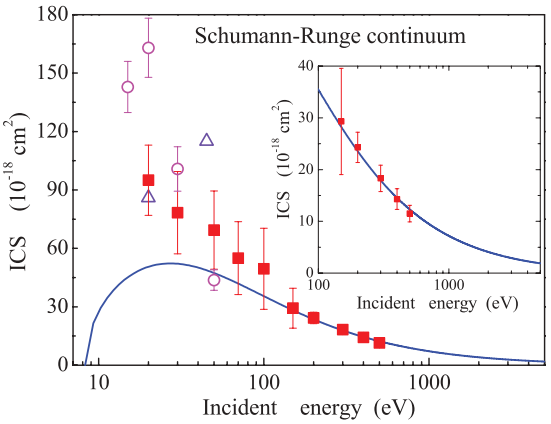

FIG. 8. (Color online) The ICS for the Schumann-Runge continuum in O_2. Solid (blue) line, the *BE*-scaled ICS. The experimental results are as follows: open (purple) triangle, Trajmar *et al.* [12]; solid (red) squares, Wakiya [23]; open (magenta) circles, Shyn *et al.* [25].

present work and Wakiya [13] for 100–500 eV may be due to the contribution of the Schumann-Runge continuum to the Herzberg pseudocontinuum in the work of Wakiya [13] as discussed previously. Another reason may be the FBA is not valid for the Herzberg pseudocontinuum and the transition of $A\ ^3\Sigma_u^+ \leftarrow X\ ^3\Sigma_g^-$ has noticeable contribution at the impact energies of 100–500 eV. As for the $O_2^-(^2\Pi_g)$ resonance in the ICS of the Herzberg pseudocontinuum, it was discussed in detail by Trajmar *et al.* [12], Teillet-Billy *et al.* [14], Green *et al.* [17], Noble and Burke [20], and Higgins *et al.* [21]. Here we do not give a superfluous discussion. It should be emphasized that the contribution from indirect processes such as the two-step virtual excitations to the Herzberg pseudocontinuum can be neglected since there is no strong dipole-allowed transition below it.

The present *BE*-scaled ICSs for the Schumann-Runge continuum are shown in Fig. 8 along with the previous experimental results [12,23,25]. It is clearly seen from Fig. 8 that the present *BE*-scaled ICSs are in excellent agreement with the data of Wakiya [23] for the incident electron energies of 100−500 eV. However, the present *BE*-scaled ICSs are lower than the results of Trajmar *et al.* [12], Wakiya [23], and Shyn *et al.* [25] at the low-incident electron energies ($E_0 < 100$ eV) except one point. The discrepancies of the

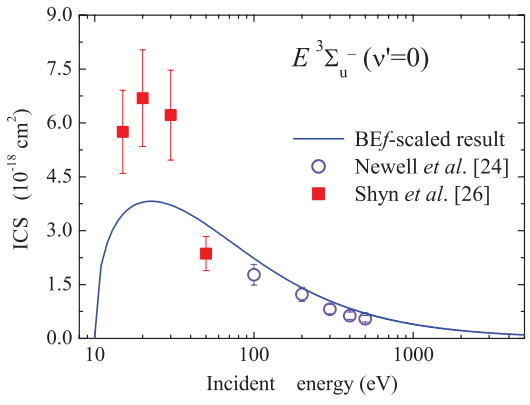

FIG. 9. (Color online) The ICS for the $E\ ^3\Sigma_u^-(v' = 0)$ state in O_2.

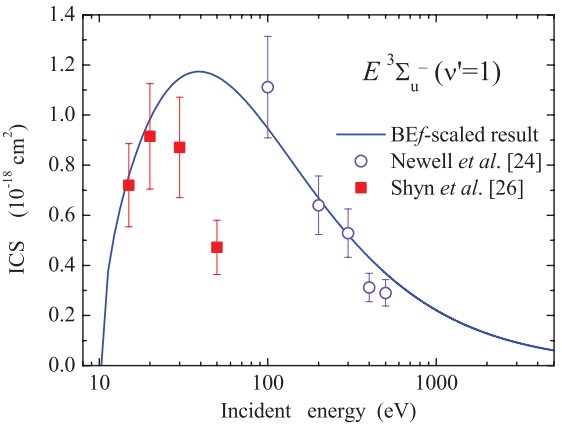

FIG. 10. (Color online) The ICS for the $E\ ^3\Sigma_u^-(v' = 1)$ state in O_2.

BE-scaled ICSs and the results of Trajmar *et al.* [12], Wakiya [23], and Shyn *et al.* [25] for $E_0 < 100$ eV may be due to the contributions from the dipole-forbidden transitions. Actually, several vibrational bands, which were observed and assigned to the $3s\sigma_g\ ^3\Pi_g$ and $^1\Pi_g$ excitations by Trajmar *et al.* [45] at residual electron energies of 0.2–7 eV, are superimposed on the Schumann-Runge continuum. And it is noticed that the spin-exchange transition of $3s\sigma_g\,^1\Pi_g \leftarrow X\ ^3\Sigma_g^-$ are much stronger than the $3s\sigma_g\ ^3\Pi_g \leftarrow X\ ^3\Sigma_g^-$ transition. The early data of Trajmar *et al.* [12] are less credible because the reliable elastic DCSs are lacking at that time and their normalization procedure is approximate.

The present *BEf*-scaled ICSs for the transitions of $E\ ^3\Sigma_u^-(v' = 0,1) \leftarrow X\ ^3\Sigma_g^-$ are shown in Figs. 9 and 10 along with the previous experimental results [24,26]. Herein the experimental ICSs of Newell *et al.* [24] were calculated by this work from their published data by fitting and integrating their apparent GOSs using Eqs. (2)–(5). Since now the more accurate optical oscillator strengths [42] are available compared with 30 years ago, the calculated ICSs of Newell *et al.* [24] were corrected by multiplying them with the ratios of f_{accu}/f_0. Herein, f_{accu} are taken from the Ref. [42] and f_0 are the fitted parameters from Eq. (2). It can be seen from Fig. 9 that the present *BEf*-scaled ICSs of the $E\ ^3\Sigma_u^-(v' = 0)$ state are lower than the ones of Shyn *et al.* [26] for 15 eV $\leqslant E_0 \leqslant$ 30 eV, while the former is higher than the latter at 50 eV. Considering the 20% error of the present *BEf*-scaled ICSs, the agreement between our results and the previous ones of Shyn *et al.* [26] is reasonable. As shown in Fig. 10, the agreement between the present *BEf*-scaled ICSs and the ones of Shyn *et al.* [26] for the transition of $E\ ^3\Sigma_u^-(v' = 1) \leftarrow X\ ^3\Sigma_g^-$ is better. It can also be seen from Figs. 9 and 10 that the experimental ICSs of Newell *et al.* [24] are in good agreement with the present results. Here, the results of Trajmar *et al.* [12] are not shown because of their approximate normalization scheme and large uncertainty as discussed previously.

IV. CONCLUSIONS

The DCSs and GOSs for electron-impact excitation of the $A'\ ^3\Delta_u$, Schumann-Runge continuum, and $E\ ^3\Sigma_u^-(v' = 0,1)$ states in O_2 have been determined at the incident electron energy of 2.5 keV and an energy resolution of 100 meV.

Compared with the low- or moderate-energy electron impact, the transition of $A'\,^3\Delta_u \leftarrow X\,^3\Sigma_g^-$ dominates the Herzberg pseudocontinuum in the present work, and its GOS was reported for the first time. It is found that the present GOSs for electron-impact excitation of the Schumann-Runge continuum and $E\,^3\Sigma_u^-(v'=1)$ are in excellent agreement with the previous results measured at incident electron energies larger than 400 eV [23,24], which indicates that the FBA is satisfied at $E_0 > 400$ eV. However, there are large discrepancies between the present GOSs and the previous ones for electron-impact excitation of the $A'\,^3\Delta_u$ and $E\,^3\Sigma_u^-(v'=0)$ states, the possible reasons for the $A'\,^3\Delta_u$ state may come from the contribution of the transition of $A\,^3\Sigma_u^+ \leftarrow X\,^3\Sigma_g^-$. More investigations for the $A'\,^3\Delta_u$ state at higher (3–4 keV) and lower (0.5–1 keV) impact energies or by the inelastic x-ray scattering method [46], which is helpful to elucidate the validity or not of the FBA, are greatly recommended. Furthermore, the calculated GOS profiles for the $E\,^3\Sigma_u^-(v'=0,1)$ by Li *et al.* [4] and Dillon *et al.* [6] are in good agreement with the experimental ones, but the calculated absolute values are much larger than the experimental data.

Based on the present GOSs of electron-impact excitation of the $A'\,^3\Delta_u$, Schumann-Runge continuum, and $E\,^3\Sigma_u^-(v'=0,1)$ states, the *BE*- or *BEf*-scaled ICSs for these states were calculated from its threshold to 5 keV. It is found the present scaled ICSs for the Schumann-Runge continuum and $E\,^3\Sigma_u^-(v'=0,1)$ are in good agreement with the previous experimental ones for electron-impact energies larger than 100 eV, while the present *BE*-scaled ICSs for the $A'\,^3\Delta_u$ state are much lower than the previous experimental ones, even for $E_0 > 100$ eV. So, further investigations about the DCSs, GOSs, and ICSs for the valance-shell excitation of oxygen, especially for the $A'\,^3\Delta_u$ and $E\,^3\Sigma_u^-(v'=0)$ states, are greatly recommended.

ACKNOWLEDGMENTS

Support of this work from the National Nature Science Foundation of China (Grants No. 10734040, No. 10874168, and No. 10979040), CAS Knowledge Promotion Project (Grant No. KJCS1-YW-N30), and National Basic Research Program of China (Grant No. 2010CB923301) are gratefully acknowledged.

[1] M. Nicolet and W. Peetermans, Planet. Space Sci. **28**, 85 (1980).
[2] M. G. Mylnczak, Geophys. Res. Lett. **23**, 657 (1996).
[3] M. J. Brunger and S. J. Buckman, Phys. Rep. **357**, 215 (2002).
[4] Y. Li, M. Honigmann, K. Bhanuprakash, G. Hirsch, R. J. Buenker, M. A. Dillon, and M. Kimura, J. Chem. Phys. **96**, 8314 (1992).
[5] M. Kimura, M. A. Dillon, R. J. Buenker, G. Hirsch, Y. Li, and L. Chantranupong, Z. Phys. D **38**, 165 (1996).
[6] M. Dillon, M. Kimura, R. J. Buenker, G. Hirsch, Y. Li, and L. Chantranupong, J. Chem. Phys. **102**, 1561 (1995).
[7] B. R. Lewis, J. P. England, S. T. Gibson, M. J. Brunger, and M. Allan, Phys. Rev. A **63**, 022707 (2001).
[8] M. Inokuti, Rev. Mod. Phys. **43**, 297 (1971).
[9] H. Bethe, Ann. Phys. **397**, 325 (1930).
[10] H. Bethe, Z. Phys. **76**, 293 (1932).
[11] K. H. Sze, C. E. Brion, X.-M. Tong, and J.-M. Li, Chem. Phys. **115**, 433 (1987).
[12] S. Trajmar, W. Williams, and A. Kuppermann, J. Chem. Phys. **56**, 3759 (1972).
[13] K. Wakiya, J. Phys. B: At. Mol. Opt. Phys. **11**, 3931 (1978).
[14] D. Teillet-Billy, L. Malegat, J. P. Gauyacq, R. Abouaf, and C. Benoit, J. Phys. B: At. Mol. Opt. Phys. **22**, 1095 (1989).
[15] M. Allan, J. Phys. B: At. Mol. Opt. Phys. **28**, 5163 (1995).
[16] L. Campbell, M. A. Green, M. J. Brunger, P. J. O. Teubner, and D. C. Cartwright, Phys. Rev. A **61**, 022706 (2000).
[17] M. A. Green, P. J. O. Teubner, M. J. Brunger, D. C. Cartright, and L. Campbell, J. Phys. B: At. Mol. Opt. Phys. **34**, L157 (2001).
[18] M. A. Green, T. Maddern, M. J. Brunger, L. Campbell, D. C. Cartright, W. R. Newell, and P. J. O. Teubner, J. Phys. B: At. Mol. Opt. Phys. **35**, 3793 (2002).
[19] T. W. Shyn and C. J. Sweeney, Phys. Rev. A **62**, 022711 (2000).
[20] C. J. Noble and P. G. Burke, Phys. Rev. Lett. **68**, 2011 (1992).
[21] K. Higgins, C. J. Noble, and P. G. Burke, J. Phys. B: At. Mol. Opt. Phys. **27**, 3203 (1994).
[22] E. N. Lassettre, S. M. Silverman, and M. E. Krasnow, J. Chem. Phys. **40**, 1261 (1964).
[23] K. Wakiya, J. Phys. B: At. Mol. Opt. Phys. **11**, 3913 (1978).
[24] W. R. Newell, M. A. Khakoo, and A. C. H. Smith, J. Phys. B: At. Mol. Opt. Phys. **13**, 4877 (1980).
[25] T. W. Shyn, C. J. Sweeney, A. Grafe, and W. E. Sharp, Phys. Rev. A **50**, 4794 (1994).
[26] T. W. Shyn, C. J. Sweeney, and A. Grafe, Phys. Rev. A **49**, 3680 (1994).
[27] K. Z. Xu, R. F. Feng, S. L. Wu, Q. Ji, X. J. Zhang, Z. P. Zhong, and Y. Zheng, Phys. Rev. A **53**, 3081 (1996).
[28] X. J. Liu, L. F. Zhu, X. M. Jiang, Z. S. Yuan, B. Cai, X. J. Chen, and K. Z. Xu, Rev. Sci. Instrum. **72**, 3357 (2001).
[29] L. F. Zhu, H. D. Cheng, Z. S. Yuan, X. J. Liu, J. M. Sun, and K. Z. Xu, Phys. Rev. A **73**, 042703 (2006).
[30] H. D. Cheng, L. F. Zhu, Z. S. Yuan, X. J. Liu, J. M. Sun, W. C. Jiang, and K. Z. Xu, Phys. Rev. A **72**, 012715 (2005).
[31] L. L. Fan, Z. P. Zhong, L. F. Zhu, X. J. Liu, Z. S. Yuan, J. M. Sun, and K. Z. Xu, Phys. Rev. A **71**, 032704 (2005).
[32] D. M. P. Holland, D. A. Shaw, S. M. McSweeney, M. A. MacDonald, A. Hopkirk, and M. A. Hayes, Chem. Phys. **173**, 315 (1993).
[33] W. B. Li, L. F. Zhu, X. J. Liu, Z. S. Yuan, J. M. Sun, H. D. Cheng, Z. P. Zhong, and K. Z. Xu, Phys. Rev. A **67**, 062708 (2003).
[34] L. F. Zhu, Z. P. Zhong, X. J. Liu, R. F. Feng, X. J. Zhang, and K. Z. Xu, J. Phys. B: At. Mol. Opt. Phys. **32**, 4897 (1999).
[35] X. Y. Han and J. M. Li, Phys. Rev. A **74**, 062711 (2006).
[36] X. J. Liu, L. F. Zhu, Z. S. Yuan, W. B. Li, H. D. Cheng, J. M. Sun, and K. Z. Xu, J. Electron Spectrosc. Relat. Phenom. **135**, 15 (2004).
[37] E. N. Lassettre, J. Chem. Phys. **43**, 4479 (1965).

[38] K. N. Klump and E. N. Lassettre, J. Chem. Phys. **68**, 886 (1978).
[39] A. R. P. Rau and U. Fano, Phys. Rev. **162**, 68 (1967).
[40] L. Vriens, Phys. Rev. **160**, 100 (1967).
[41] Y. K. Kim, J. Chem. Phys. **126**, 064305 (2007).
[42] W. F. Chan, G. Cooper, and C. E. Brion, Chem. Phys. **170**, 99 (1993).
[43] Y. K. Kim, Phys. Rev. A **64**, 032713 (2001).
[44] D. C. Cartwright, S. Trajmar, W. Williams, and D. L. Huestis, Phys. Rev. Lett. **27**, 704 (1971).
[45] S. Trajmar, D. C. Cartwright, and R. I. Hall, J. Chem. Phys. **65**, 5275 (1976).
[46] B. P. Xie, L. F. Zhu, K. Yang, B. Zhou, N. Hiraoka, Y. Q. Cai, Y. Yao, C. Q. Wu, E. L. Wang, and D. L. Feng, Phys. Rev. A **82**, 032501 (2010).